10-13-2022

# Tunable Electronic Structure via DNA-Templated Heteroaggregates of Two Distinct Cyanine Dyes

Jonathan S. Huff
*Boise State University*

Matthew S. Barclay
*Boise State University*

Azhad U. Chowdhury
*Boise State University*

Lance K. Patten
*Boise State University*

Simon K. Roy
*Boise State University*

*See next page for additional authors*

## Publication Information

Huff, Jonathan S.; Díaz, Sebastián A.; Barclay, Matthew S.; Chowdhury, Azhad U.; Chiriboga, Matthew; Ellis, Gregory A.; . . . and Pensack, Ryan D. (2022). "Tunable Electronic Structure via DNA-Templated Heteroaggregates of Two Distinct Cyanine Dyes". *The Journal of Physical Chemistry C, 126*(40), 17164-17175. https://doi.org/10.1021/acs.jpcc.2c04336

THE JOURNAL OF PHYSICAL CHEMISTRY C
A JOURNAL OF THE AMERICAN CHEMICAL SOCIETY

pubs.acs.org/JPCC

Article

# Tunable Electronic Structure via DNA-Templated Heteroaggregates of Two Distinct Cyanine Dyes

Jonathan S. Huff, Sebastián A. Díaz, Matthew S. Barclay, Azhad U. Chowdhury, Matthew Chiriboga, Gregory A. Ellis, Divita Mathur, Lance K. Patten, Simon K. Roy, Aaron Sup, Austin Biaggne, Brian S. Rolczynski, Paul D. Cunningham, Lan Li, Jeunghoon Lee, Paul H. Davis, Bernard Yurke, William B. Knowlton, Igor L. Medintz, Daniel B. Turner,* Joseph S. Melinger,* and Ryan D. Pensack*

Cite This: *J. Phys. Chem. C* 2022, 126, 17164−17175

Read Online

ACCESS | Metrics & More | Article Recommendations | Supporting Information

**ABSTRACT:** Molecular excitons are useful for applications in light harvesting, organic optoelectronics, and nanoscale computing. Electronic energy transfer (EET) is a process central to the function of devices based on molecular excitons. Achieving EET with a high quantum efficiency is a common obstacle to excitonic devices, often owing to the lack of donor and acceptor molecules that exhibit favorable spectral overlap. EET quantum efficiencies may be substantially improved through the use of heteroaggregates—aggregates of chemically distinct dyes—rather than individual dyes as energy relay units. However, controlling the assembly of heteroaggregates remains a significant challenge. Here, we use DNA Holliday junctions to assemble homo- and heterotetramer aggregates of the prototypical cyanine dyes Cy5 and Cy5.5. In addition to permitting control over the number of dyes within an aggregate, DNA-templated assembly confers control over aggregate composition, i.e., the ratio of constituent Cy5 and Cy5.5 dyes. By varying the ratio of Cy5 and Cy5.5, we show that the most intense absorption feature of the resulting tetramer can be shifted in energy over a range of almost 200 meV (1600 $cm^{-1}$). All tetramers pack in the form of H-aggregates and exhibit quenched emission and drastically reduced excited-state lifetimes compared to the monomeric dyes. We apply a purely electronic exciton theory model to describe the observed progression of the absorption spectra. This model agrees with both the measured data and a more sophisticated vibronic model of the absorption and circular dichroism spectra, indicating that Cy5 and Cy5.5 heteroaggregates are largely described by molecular exciton theory. Finally, we extend the purely electronic exciton model to describe an idealized J-aggregate based on Förster resonance energy transfer (FRET) and discuss the potential advantages of such a device over traditional FRET relays.

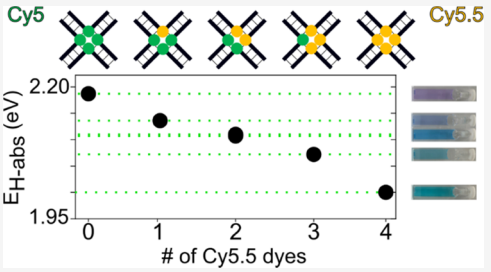


## INTRODUCTION

Molecular excitons are essential to applications in light harvesting,[1,2] organic optoelectronics,[3] and nanoscale computing.[4−10] In light harvesting and organic optoelectronics, for example, solar photons are converted into molecular excitons that undergo several energy-transfer steps from the site of initial photoexcitation to the reaction center or charge-transfer interface where they are converted into reaction products or photocurrent. In nanoscale computing, molecular excitons carry information and propagate between optical inputs, active elements (such as logic gates), and optical outputs via energy transfer. Each of these applications requires an overall high efficiency, and therefore each step needs to be as efficient as possible. Thus, strategies to increase the efficiency of energy-transfer steps are desirable to improve the overall performance.

There are several parameters that determine the efficiency of electronic energy transfer (EET) of molecular excitons, which leads to a number of approaches to improve EET efficiency. At the most general level, the efficiency of EET depends on kinetic competition between the rate of EET and the rate of excited-state decay. Therefore, EET efficiency can be improved by increasing the rate of EET or by decreasing the rate of excited-state decay. The rate of EET is the rate at which an exciton on a donor incoherently hops to a nearby, unexcited acceptor. The rate of EET, which, in certain limits, is described by Förster resonance energy transfer (FRET),[11−15] depends on the coupling strength between the donor and the acceptor along with the overlap between the donor emission and the acceptor absorption spectra.[13,16,17] Thus, the rate of EET can be increased by increasing the coupling strength between the donor and the acceptor. However, this approach has practical limits as FRET is only applicable in the limit of weak coupling. Another way in which the rate of EET can be increased is by improving the spectral overlap of the donor and acceptor. For

Received: June 22, 2022
Revised: September 8, 2022
Published: September 28, 2022

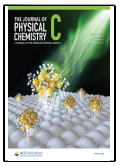





https://doi.org/10.1021/acs.jpcc.2c04336
*J. Phys. Chem. C* 2022, 126, 17164−17175

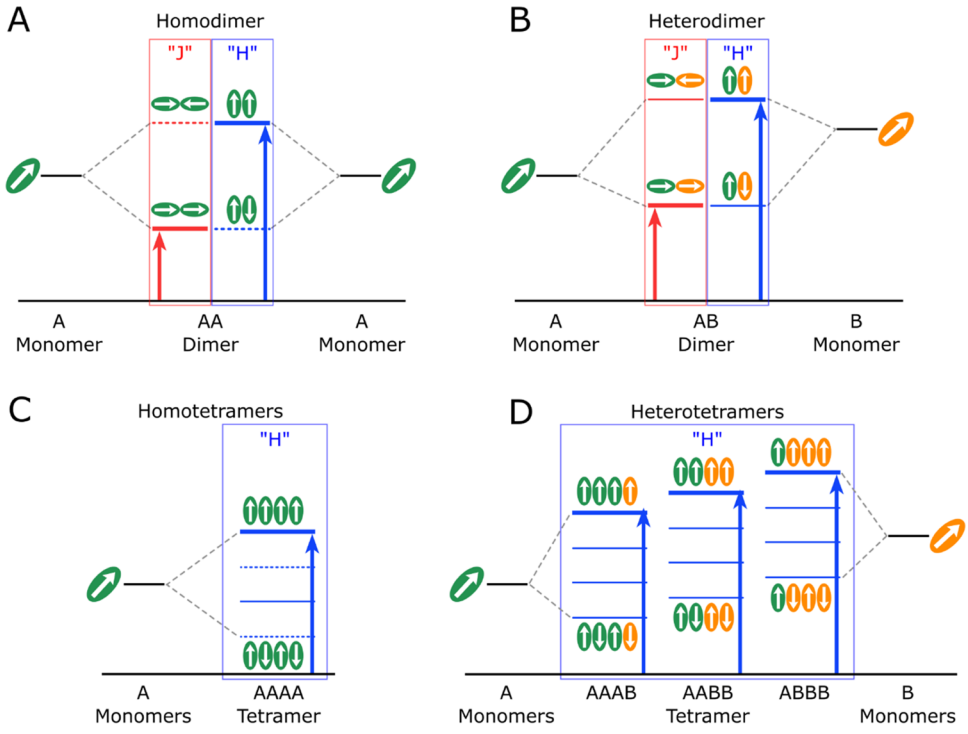


**Figure 1.** Energy-level diagrams depicting monomer electronic states and associated dimer and tetramer aggregate excitonic states. (A) Energy-level diagram for an ideal molecular dimer composed of two identical monomers, i.e., a homodimer, packing in the form of J- and H-aggregates. As a result of excitonic coupling between the two monomers, two new excitonic states are formed with energies and transition dipole moment (TDM) amplitudes dependent on the geometric arrangement of the monomers. The monomers comprising the dimer are represented as green ovals and include TDM vectors as white arrows along the molecular long axis (i.e., assuming a rod-like shape for the molecule). There are two distinct packing arrangements for J- and H-aggregates, resulting in four total distinct packing arrangements. A cartoon schematic for each of these packing arrangements, i.e., the geometric arrangement of the monomers, is shown next to the corresponding excitonic state. Excitonic states able and unable to optically couple to the ground state are depicted as thick solid lines and thin dashed lines, respectively. The higher- and lower-energy excitonic transitions are forbidden for J- and H-aggregates, respectively. Optically allowed transitions are shown as red and blue arrows. (B) Energy-level diagram for an ideal molecular dimer composed of two different monomers, i.e., a heterodimer, packing in the form of J- and H-aggregates. The TDMs of monomers A and B are represented as white vectors enclosed in green and orange ovals, respectively. As in the homodimer, excitonic coupling between the two monomers produces two new excitonic states, but, due to the nature of heteroaggregate coupling, the transitions to the optically forbidden states become weakly allowed in heteroaggregates and are shown as thin solid lines. Because there is only one composition for the heterodimer, i.e., AB, there is no ability to further tune the energies of these states. (C) Energy-level diagram for an ideal molecular tetramer composed of four identical monomers, i.e., a homotetramer, packing in the form of an H-aggregate. As a result of excitonic coupling between the four monomers, four new excitonic states result. For ease of viewing, the geometric arrangement of the monomers is only shown for the highest and lowest energy states. (D) Energy-level diagram for an ideal molecular tetramer composed of two different monomers, i.e., a heterotetramer, packing in the form of an H-aggregate. Excitonic coupling between the four monomers produces four new excitonic states; as in the case of the heterodimer, the optical transitions that are forbidden in the homotetramer (i.e., the three lower-energy states) are weakly allowed. Because there are three different compositions for the heterotetramer, i.e., AAAB, AABB, and ABBB, the energies of the heterotetramer excitonic states can be tuned. Specifically, by adjusting the ratio of the two monomers comprising the heterotetramer, the excitonically split states can be tuned to higher or lower energies.

example, dyes can be chemically modified to alter their electronic structure for improved spectral overlap. Chemically modifying the dye structure, however, can be challenging in the case where several successive steps are necessary to achieve long-range spatial separation of the electronic excitation energy. An alternative approach is to use molecular dye aggregates as the building blocks for long-range and spatially directed energy transfer. The transition energies of dye aggregates can be tuned and they can exhibit more intense absorption and emission, both of which are desirable for improving spectral overlap.[18,19] Examples of rapid long-range and spatially directed energy transfer facilitated by aggregates can be found in nature in the photosynthetic light-harvesting complexes of certain extremophile bacteria.[20]

One way to tune the electronic structure is by assembling aggregates of one type of dye and modifying their packing. Dye packing determines the orientation of the constituent dye transition dipole moments (TDMs), which in turn governs the aggregate's transition energies and absorption and emission intensity.[21−24] For example, when TDMs orient in an end-to-end configuration, the resulting J-aggregate energy levels split and the absorption intensity is redistributed to the lower-energy transition, leading to red-shifted absorption features relative to the monomer (Figure 1A). Similarly, when TDMs orient face-to-face in a H-aggregate configuration, the absorption intensity is redistributed to the higher-energy transition, resulting in blue-shifted absorption features.

An alternative, albeit less explored, way of tuning the electronic structure is by assembling aggregates of two chemically distinct dyes. It is instructive to first consider the case where we have two homoaggregate dimers corresponding to two chemically distinct dyes, which, for simplicity, we


https://doi.org/10.1021/acs.jpcc.2c04336
J. Phys. Chem. C 2022, 126, 17164−17175

**Scheme 1. Chemical Structures of Dual-Phosphoramidite-Functionalized Cy5 and Cy5.5 (Top) and Schematic Illustrations of Cy5 and Cy5.5 Homo- and Heterotetramer Aggregates Templated Using DNA Holliday Junctions (Bottom)[a]**

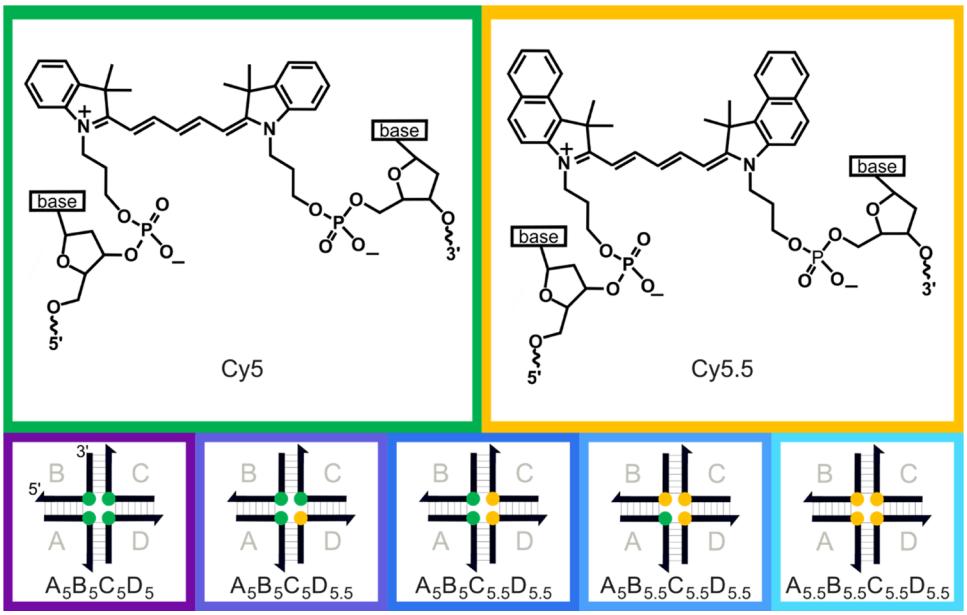


[a]Cy5 and Cy5.5 are represented as green and yellow circles, respectively. The DNA-dye constructs are composed of four dye-labeled oligonucleotide sequences, with the oligonucleotide sequences shown as black lines with the half-arrowhead pointed toward the 5′ part of the sequence and with the full sequence provided in Section S1. Gray lines between oligonucleotides represent hydrogen bonding between complementary nucleobases. The DNA-dye construct configurations include two homotetramers (i.e., $A_5B_5C_5D_5$ and $A_{5.5}B_{5.5}C_{5.5}D_{5.5}$) and three heterotetramers ($A_5B_5C_5D_{5.5}$, $A_5B_5C_{5.5}D_{5.5}$, and $A_5B_{5.5}C_{5.5}D_{5.5}$), which are a subset of the 16 total possible tetramer configurations.

assume to have identical TDMs and exhibit the same packing arrangement. In the case of J-aggregate homodimers of dyes A and B, the lowest energy optical transition of the two homodimers, AA and BB, are lower in energy compared with the transition energy of the corresponding monomer and the dimers exhibit enhanced radiative decay rates. Thus, while there is some enhancement in the radiative decay rate, there is no gain in the number of distinct transition energies (i.e., two distinct monomer transition energies compared with two distinct homodimer transition energies). Now, let us consider a third possibility—the heterodimer, AB (Figure 1B). The heterodimer will have new electronic states intermediate in energy between those of the two homodimers and, in the case of J-aggregation, maintain enhanced radiative decay rates and increased absorption intensity. In the case of the heterodimer, we now have additional electronic structure tunability without the need for a third chemically distinct dye. This concept can be extended further to higher-order aggregates such as tetramers. As in the homodimer, the homotetramer offers no gain in the number of distinct transition energies (Figure 1C). In contrast, for a set of heterotetramers consisting of different combinations of two chemically distinct dyes, five distinct transition energies are possible. Specifically, the three distinct transition energies that correspond to the heterotetramers (i.e., AAAB, AABB, and ABBB) are shown in Figure 1D, and there are two additional distinct transition energies corresponding to the two homotetramers (i.e., AAAA and BBBB). We now have added tunability—the energy difference between the distinct transition energies is smaller—meaning that we can tune electronic structure on a finer scale. It is important to mention that the possibility of assembling high-order aggregates, such as heterotetramers, is not unrealistic, as studies on methyl red aggregates,[25] merocyanine aggregates,[26] and crystalline polyacenes[27] have indicated that the spatial extent of exciton delocalization in aggregates of these dyes can encompass as many as six, eight, and ten dyes, respectively. The challenge in implementing high-order heteroaggregates thus far has not been the spatial extent of exciton delocalization—rather, it has been in controlling their assembly.

A promising way of assembling heteroaggregates involves harnessing the programmability and bottom-up self-assembly of DNA. Using DNA nanotechnology, oligonucleotides with specific sequences can be designed to self-assemble into a variety of low-dimensional structures such as multi-armed junctions,[28] dendrimers,[29] hairpins,[30] and loops.[31] Much larger DNA structures with sizes on the order of hundreds of nanometers have also been realized through DNA origami,[32] and similarly large vesicles, ribbons, and star-shaped structures have been self-assembled using chemically modified, amphiphilic duplex DNA where the ends are hydrophobic and the interior is hydrophilic.[33,34] In addition to having enormous structural diversity, DNA is amenable to a vast number of chemical modifications including dye labeling. By chemically attaching dyes to the DNA backbone, it is possible to bring dyes into close proximity at sub-nanometer separations. Through DNA templating, the aggregate size and composition can also be controlled, which are distinct advantages over solution-based assembly of aggregates. To date, DNA has been used to systematically examine the structure and dynamics of a number of strongly coupled homoaggregates,[35−44] with cyanines representing an exceptional class of dyes facilitating the assembly and characterization of excitonically coupled dye aggregates.[35,36,42,45−47] Despite the relative ease with which DNA can be used to assemble heteroaggregates, only a very small subset of studies on DNA-templated dye aggregates have included heteroaggregates.[46,48−50] Further, these studies largely


https://doi.org/10.1021/acs.jpcc.2c04336
J. Phys. Chem. C 2022, 126, 17164−17175

focused on the steady-state optical properties and electronic structure of the DNA-templated heteroaggregates, without details of the excited-state dynamics.

In this work, we show how to systematically tune the electronic structure in a series of DNA-templated tetramer aggregates by varying the aggregate composition. We use Cy5 and Cy5.5, two chemically distinct and prototypical dyes used in excitonics and imaging, and assemble the dyes into a series of homo- and heterotetramer aggregates (Scheme 1). We chose these specific dyes for their compatibility, which arises from their similar chemical structures, large transition dipole moment amplitudes,[51] overall similar optical spectra (in spectral range and shape),[43] and their facile incorporation into DNA oligonucleotides.[52] Using steady-state absorption and circular dichroism (CD) spectroscopy, we find that all of the tetramers exhibit strong excitonic interactions and that the constituent dyes pack in the form of H-aggregates. Remarkably, as the composition of the tetramer is varied, i.e., by increasing the Cy5.5 content, we observe a progressive shift of the primary absorption band to longer wavelengths over an energy span of ∼200 meV (∼1600 $cm^{-1}$). We find via steady-state fluorescence measurements that all of the tetramers exhibit quenched fluorescence. This result, combined with a more than tenfold reduction in excited-state lifetimes of the tetramers compared to the monomers as measured via transient absorption, indicates that the tetramers exhibit enhanced nonradiative decay relative to the monomers. We use a purely electronic model based on molecular exciton theory to explain the progression of the most intense and highest energy absorption band of each homo- and heterotetramer aggregate. In parallel, we simulate the steady-state absorption and CD spectra via an approach based on the Kühn−Renger−May (KRM) theory, which includes one vibronic mode and produces a packing configuration and excitonic interaction strengths similar to the purely electronic model. We conclude by applying the model to an idealized energy-transfer relay based on a series of J-aggregate homo- and heterotetramers, which can transfer electronic excitation energy over a large spatial distance (16 nm) with high quantum efficiency (99.9%).

## RESULTS AND DISCUSSION

**Electronic Structure Characterization via Steady-State Absorption and Circular Dichroism.** We first used steady-state absorption spectroscopy to characterize the electronic structure of Cy5 and Cy5.5 monomers attached to DNA Holliday junctions. Section S1 includes details of the oligonucleotide labeling and assembly of the DNA Holliday junctions. Absorption spectra are shown in Figure 2A. The monomer spectra resemble one another and are characterized by a prominent lowest energy absorption band, with less intense vibronic shoulders at shorter wavelengths. The absorption maximum, which we assign to the 0−0 absorption band, is located at ca. 653 and 695 nm for Cy5 and Cy5.5, respectively. The presence of additional aryl groups on Cy5.5 extends the size of the conjugated network compared to Cy5 and results in the overall red-shifted absorption spectrum. For both dyes, the next most intense (i.e., 0−1) absorption band is shifted in energy by ∼1100 $cm^{-1}$ (∼140 meV), indicating that the electronic transition is coupled to a symmetric CC stretching mode.[53,54] The 0−1 absorption band is more intense for the Cy5.5 monomer, indicating that the displacement between the ground and lowest energy excited electronic

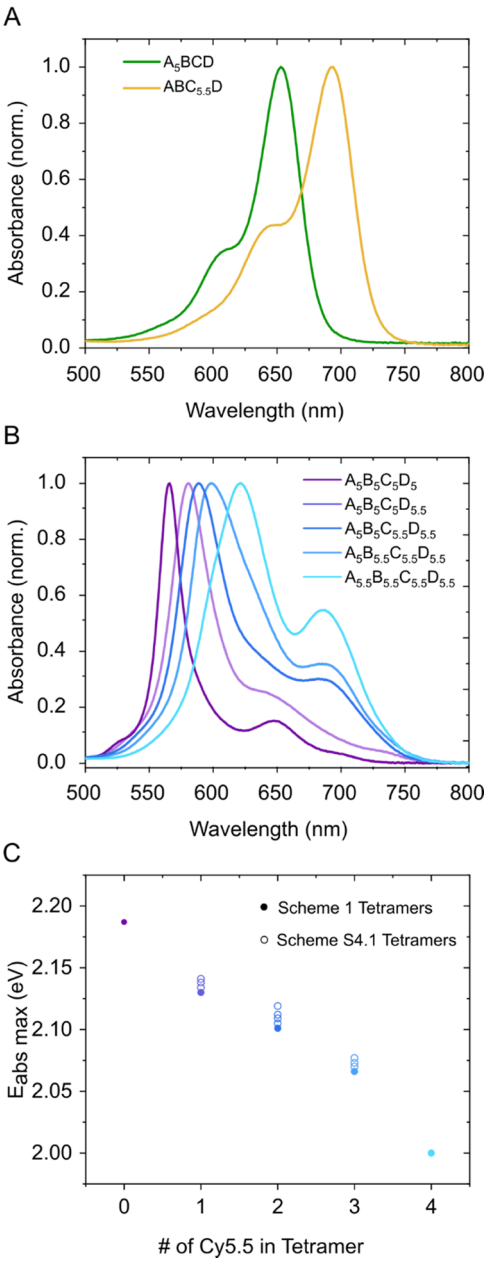


**Figure 2.** Steady-state absorption spectra of the DNA-templated monomer and heterotetramer structures shown in Scheme 1. (A) Steady-state absorption spectra of representative Cy5 and Cy5.5 monomers. The absorption spectra of all monomer configurations are plotted in Section S2. (B) Steady-state absorption spectra of the Cy5−Cy5.5 homo- and heterotetramers. (C) Energy of the peak of the most intense absorption band appearing in the spectra of the homo- and heterotetramers displayed as a function of Cy5.5 content. Closed circles correspond to the most intense absorption band of the five homo- and heterotetramer configurations shown in Scheme 1 (and plotted in panel B), while open circles correspond to the remaining 11 heterotetramer configurations shown in Section S5.

potential energy surfaces (i.e., $S_0$ and $S_1$) is greater for Cy5.5 than for Cy5. An important precursor for excitonic interactions (and delocalization) is the transition dipole moment (TDM) amplitude.[22] To gain insight into the magnitude of the TDM of the monomers, we measured their extinction spectra. The extinction spectra are useful in this regard because the peak extinction coefficient is generally proportional to the TDM



https://doi.org/10.1021/acs.jpcc.2c04336
J. Phys. Chem. C 2022, 126, 17164−17175

amplitude.[24] The results indicate that Cy5 and Cy5.5 have peak extinction coefficients of ∼239 000 and ∼230 000 $M^{-1}$ $cm^{-1}$, respectively, with these values representing the average of the peak extinction coefficient of the monomers attached to each of the four strands of the Holliday junction (Section S2). Such large peak extinction coefficients (and similar absorption profiles) are consistent with the large calculated TDM amplitudes of Cy5 and Cy5.5 of ∼15−16 D.[51,55,56] Taken together, the results suggest that Cy5 and Cy5.5 are capable of strong excitonic interactions when brought into close proximity (i.e., sub-nanometer intermolecular separation).

Figure 2B displays the steady-state absorption spectra of five different homo- and heterotetramer aggregates of Cy5 and Cy5.5. In the case of the Cy5 and Cy5.5 homotetramers, we observe that their absorption spectra are drastically different than those of the Cy5 and Cy5.5 monomers. Specifically, in both cases, we observe (i) an intense primary absorption band blue-shifted relative to the monomers, which is indicative of strong excitonic interactions between dyes and (ii) an overall blue shift of the absorption profile, which indicates the dyes are packing in a primarily face-to-face, or H-aggregate, arrangement. Additionally, we find that the most intense absorption band of the Cy5.5 homotetramer is considerably broader than the corresponding absorption band of the Cy5 homotetramer. We also measured the circular dichroism (CD) spectra of the Cy5 and Cy5.5 homotetramers, which provide additional evidence for strong excitonic interactions between dyes (Section S3). Specifically, the monomer CD spectra are featureless in the visible range, while the tetramer CD spectra exhibit intense positive and negative peaks in the same spectral region. The positions of the CD features in the Cy5 homotetramer at ∼569 and 701 nm are consistent with a prior report;[57] the CD features in the Cy5.5 homotetramer are consistent with the interpretation of strong excitonic interactions between dyes and indicate that the additional steric bulk via the introduction of the phenyl rings does not compromise these strong excitonic interactions.

Motivated by the evidence of strong excitonic interactions in the homotetramers, we proceeded to assemble and characterize a series of Cy5 and Cy5.5 heterotetramer aggregates (Figure 2B). In the series, we successively substitute Cy5.5 dyes with Cy5 dyes to result in the following heterotetramers: $A_5B_5C_5D_{5.5}$, $A_5B_5C_{5.5}D_{5.5}$, and $A_5B_{5.5}C_{5.5}D_{5.5}$. Remarkably, just as we saw for the homotetramers, we also observe drastic spectral changes for these heterotetramers, which indicates that the chemically distinct Cy5 and Cy5.5 dyes are capable of strong excitonic interactions (Section S4). Specifically, all heterotetramers exhibit an intense primary absorption that is blue-shifted relative to both the Cy5 and Cy5.5 monomer absorption maxima, indicating a common H-aggregate packing arrangement (and further indicating that the added steric bulk with successive Cy5.5 substitution does not disrupt this common packing arrangement). Additionally, we find that the absorption maxima and widths of the heterotetramers are intermediate between those of the two homotetramers with increasing Cy5.5 substitutions. Specifically, the most intense transition energy ($E$) and its associated width ($\sigma$) exhibit a gradual progression from high to low energy and narrow to broad width in the order $E_{Cy5(3)Cy5.5(1)} > E_{Cy5(2)Cy5.5(2)} > E_{Cy5(1)Cy5.5(3)}$ and $\sigma_{Cy5(3)Cy5.5(1)} < \sigma_{Cy5(2)Cy5.5(2)} < \sigma_{Cy5(1)Cy5.5(3)}$, respectively.

To investigate the generality of this effect, we characterized all possible heterotetramer configurations. In total, 14 heterotetramer configurations are possible, with three representative mono-, di-, and tri-Cy5.5 substituted configurations shown in Scheme 1. Section S5 displays the schematic of the remaining 11 heterotetramer configurations, along with the absorption spectra for all 14 heterotetramers (including those plotted in Figure 2). In all cases, i.e., mono-, di-, and tri-Cy5.5 substitution, the absorption spectra of the corresponding heterotetramers are similar. The major differences include (i) a slight energy shift of the most intense absorption band (as is evident by comparing the solid and open circles displayed in Figure 2C) and (ii) changes in absorption intensity in the vicinity of where the Cy5 and Cy5.5 monomers absorb. The former observation, combined with the observation that the dyes pack in a similar H-aggregate configuration in all cases, suggests that, while the DNA brings the dyes close, the dye packing is driven largely by self-association of the dyes, i.e., strong interdye interactions. We attribute the slight energy shift of the absorption maxima either to subtle differences in packing, which impacts the excitonic interaction strength, or to differences in the solvent environment, i.e., solvatochromism. The second observation, i.e., that the absorption intensity changes in the vicinity of where the Cy5 and Cy5.5 monomers absorb, is consistent with past observations of a small subpopulation of "optical" monomers in these materials,[58,59] which we attribute to either DNA "breathing"[60] or different packing in different DNA conformers.[39,59]

**Excited-State Electronic Structure and Dynamics.** We next proceeded to characterize the structure and dynamics of the lowest energy excited state of the homo- and heterotetramer aggregates via steady-state fluorescence spectroscopy. Much like the Cy5 homotetramer solution where extensive quenching compared to the monomer has been observed,[45,57−59] all tetramer solutions exhibit highly quenched fluorescence emission (Section S6). Such strongly quenched fluorescence emission is consistent with enhanced nonradiative decay in all of the tetramer structures. Interestingly, the fluorescence emission spectra of the heterotetramer solutions exhibit prominent emission bands peaking in the vicinity of the most intense features in the Cy5 and Cy5.5 monomer emission spectra. Furthermore, the heterotetramer solution emission spectra strongly resemble a combination of the Cy5 and Cy5.5 monomer emission spectra. As such, we assign the majority of emission coming from the heterotetramer solutions as arising from a small subpopulation of "optical" monomers, which was confirmed by performing fluorescence excitation spectroscopy measurements (Section S7). Previous work suggested that the Cy5 homotetramer solution exhibited an exceptionally weak emission band in the vicinity of ∼800 nm.[58] To determine whether the heterotetramers are emissive and, if so, the approximate spectral range of emission, we collected fluorescence emission spectra over a range of excitation wavelengths to generate fluorescence emission−excitation surface plots. These measurements indicate that the homo- and heterotetramer structures do indeed emit, albeit weakly, in the range of ∼750−850 nm (Section S7).

To gain insight into the mechanism of the enhanced nonradiative decay, we additionally performed femtosecond transient absorption (TA) spectroscopy measurements, which are capable of probing both "bright" and "dark" excited states. In the measurements, a pump pulse excites the sample and a time-delayed probe pulse measures the electronic structure of the electronically excited population. As such, different decay pathways such as direct return to the ground state, conversion


https://doi.org/10.1021/acs.jpcc.2c04336
J. Phys. Chem. C 2022, 126, 17164−17175

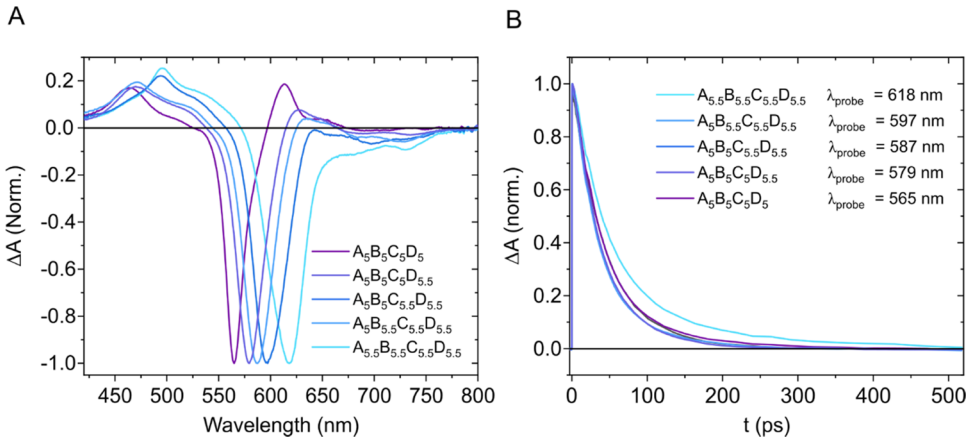


**Figure 3.** Transient absorption spectra (A) and kinetics traces (B) for a series of tetramers. The TA spectra correspond to a pump−probe delay of 3 ps. The main bleach features reflect the progression of the main steady-state absorption features. For samples $A_5B_5C_5D_5$, $A_5B_5C_5D_{5.5}$, $A_5B_5C_{5.5}D_{5.5}$, $A_5B_{5.5}C_{5.5}D_{5.5}$, and $A_{5.5}B_{5.5}C_{5.5}D_{5.5}$, the excitation wavelengths were centered at ∼565, 579, 587, 697, and 618 nm, respectively.

to triplet excitations, or conversion to charge carriers can be evaluated. Figure 3A displays the normalized TA spectra for the homo- and heterotetramer aggregate solutions excited near their respective maxima and at a time delay of 3 ps. Each spectrum exhibits an intense negative-going peak corresponding to the ground-state bleach (GSB) of the most intense absorption band. The GSB exhibits the same red-shifted progression with increased Cy5.5 content observed in the steady-state absorption spectra (Figure 2B). Much weaker GSB bands are also visible at longer wavelengths for each of the solutions, which we attribute to the weak absorption evident in the steady-state absorption. Additionally, we observe positive-going excited-state absorption (ESA) bands on both sides of the primary GSB for all of the tetramers. The ESA to the red of the primary GSB is most apparent as a positive peak at ca. 615 nm in the Cy5 homotetramer TA spectrum. With successive Cy5.5 substitution, this ESA decreases in intensity, possibly as a result of the overlapping primary GSB band, such that tracking its peak position is not possible. On the blue side of the primary GSB, the ESA bands do not follow a smooth progression. Interestingly, the peak position of the ESA band of the $A_5C_5B_5D_{5.5}$ and $A_5B_5C_{5.5}D_{5.5}$ heterotetramers at ∼460 nm largely matches that of the Cy5 homotetramer, while the peak position of the ESA band of the $A_5B_{5.5}C_{5.5}D_{5.5}$ heterotetramer at ∼500 nm largely matches that of the Cy5.5 homotetramer.

We next consider the excited-state dynamics of the tetramers. Figure 3B displays normalized kinetics traces of the decay of the primary GSB feature for each tetramer in the series. The kinetics traces all decay at a similar rate and recover to baseline within 500 ps, with no apparent relationship between the Cy5.5 content of the tetramers and the relaxation rate. The complete recovery of the GSB indicates that the entire excited-state population has returned to the ground state, suggesting that the solutions contain no long-lived "dark" populations. To determine the excited-state lifetimes of the tetramer solutions, we performed global target analysis (GTA) on the TA datasets (Section S8). GTA can be used to isolate individual spectra and decay kinetics when overlapping signals from multiple populations are embedded in a TA dataset. GTA proceeds according to a kinetic model that states the number of populations and their relationship to one another in terms of the decay pathway (i.e., parallel and sequential). For all homo- and heterotetramer TA datasets, we applied a two-component kinetic model that we previously used to model the TA of Cy5 homotetramers.[59] The two-component model includes (i) an initial component that we assign to a rapid structural relaxation process, as is evident in changes in the excited-state absorption bands and (ii) a second component that we assign to relaxation to the ground state, based on the decay of all transient spectral features including the GSB bands. The extracted lifetimes, which correspond to the second component, are listed in Table 1. Perhaps surprisingly, we observe very little variation in the excited-state lifetimes of the series, which ranges from ∼40 to 60 ps. The lifetimes of the tetramer solutions are more than an order of magnitude shorter than the monomer solutions, indicating that the excited-state quenching previously observed in homotetramers also occurs in heterotetramers.[58,59] This result, combined with the dramatically reduced fluorescence intensity of the tetramers compared to the monomers, further corroborates that the quenched fluorescence of the tetramer solutions results from rapid nonradiative decay to the ground state. We assign the nonradiative decay to a nonadiabatic transition from the lowest energy excited state ($S_1S_0$) to the ground state ($S_0S_0$), and note that such quenching has been observed in a number of additional strongly coupled dye aggregate systems.[58]

**Table 1. Excited-State Lifetimes of Cy5 and Cy5.5 Monomer and Tetramer Solutions**

| sample | $\tau$ (ps) |
|---|---|
| $A_5BCD$ | 1870 ± 20 |
| $ABC_{5.5}D$ | 920 ± 10 |
| $A_5B_5C_5D_5$ | 44.2 ± 0.6 |
| $A_5B_5C_5D_{5.5}$ | 38.3 ± 0.5 |
| $A_5B_5C_{5.5}D_{5.5}$ | 38.7 ± 0.5 |
| $A_5B_{5.5}C_{5.5}D_{5.5}$ | 45.5 ± 0.9 |
| $A_{5.5}B_{5.5}C_{5.5}D_{5.5}$ | 58.6 ± 0.5 |

**Purely Electronic Exciton Theory Model of the Electronic Structure.** The similarities in appearance between the tetramer absorption spectra (Figure 2B)—which is mirrored in the TA spectra (Figure 3A) as well as the regular progression both sets of spectra display with increasing Cy5.5 content—suggest that the dyes in each tetramer pack similarly and experience similar excitonic interactions. To better understand the observed progression of the absorption spectra,


https://doi.org/10.1021/acs.jpcc.2c04336
J. Phys. Chem. C 2022, 126, 17164−17175

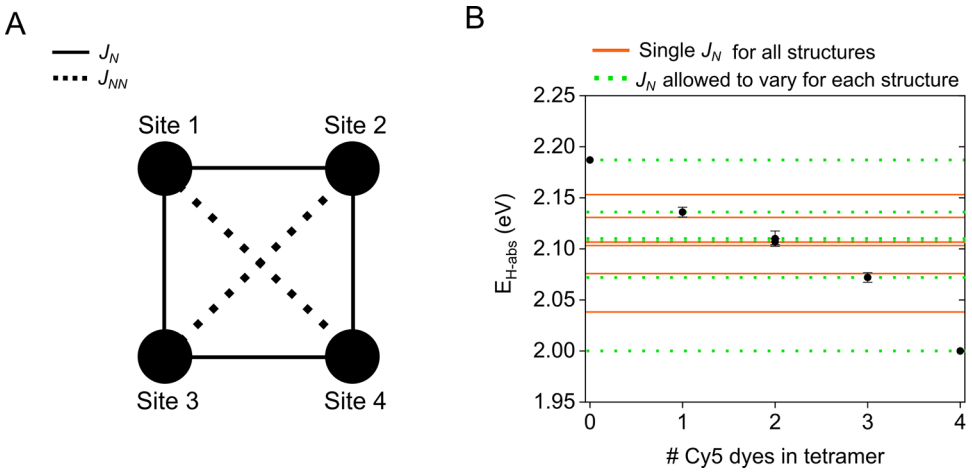


**Figure 4.** (A) Schematic illustration of the dye configuration used in the Hamiltonian. Black dots represent the TDM centers (pointing into and out of the plane of the page). Lines represent the excitonic hopping parameter between pairs of dyes. (B) Energies of the blue-shifted absorption maxima of the DNA Holliday junction-templated tetramer solutions as a function of Cy5.5 content (circles), and corresponding best fits of the highest energy eigenvalue (horizontal lines) calculated from exciton theory using a single value for the exciton hopping parameter, $J_N$, as the only fitting parameter (orange lines), and allowing $J_N$ to vary for each structure (green dotted lines). The error bars represent the variance of the absorption maxima for tetramers of a given composition. Two circles and fit lines are plotted for the tetramers composed of two Cy5 and two Cy5.5 molecules because of the two distinct symmetries associated with placing the like dyes at adjacent corners or across the diagonal of a square. The full set of calculated energy eigenvalues for the global and individual fits is listed in Section S10.

we use a model based on Kasha's molecular exciton theory to predict the progression.[21−23] We made several assumptions to create a model Hamiltonian. We first assumed that the dyes were located at the four corners of a square with their TDMs aligned parallel to one another and normal to the plane of the square, which prior studies have indicated is approximately representative.[45] We additionally assumed that excitonic interactions between pairs of dyes, described quantitatively by the excitonic hopping parameter, $J_{mn}$, are independent of the dye type. We were motivated to make this assumption as the excitonic interactions between pairs of dyes are mediated by their TDM, which seemed reasonable given that the TDMs of Cy5 and Cy5.5 are similar.[51,55,56] Finally, we assumed that excitonic interactions between dyes were mediated purely by electronic coupling; that is, vibronic coupling was neglected. The assumption here is reasonable, given the considerable amplitude of the dye TDMs, which is associated with a fully allowed electronic transition. These assumptions yield a diagonally symmetric 4 × 4 Hamiltonian matrix. In the Hamiltonian, we assume a single value for the excitonic hopping parameter associated with nearest-neighbor dyes, which we label $J_N$. Likewise, we assume a single value for the excitonic hopping parameter associated with next-nearest-neighbor dyes interacting across the diagonal, which we label $J_{NN}$, and further assume that $J_{NN} = 2^{-3/2} \times J_N$ due to the $R^3$ dependence of $J_{mn}$ on dye separation. The relationship between $J_N$ and $J_{NN}$ is represented schematically in Figure 4A. Assuming periodic boundary conditions, the Hamiltonian for such a tetramer is given by

$$\hat{H} = \sum_{j=0}^{3} \varepsilon_i |i\rangle\langle i| + \sum_{j=i\pm1}^{3} J_N |j\rangle\langle i| + \sum_{j=i\pm2}^{3} 2^{-3/2} J_N |j\rangle\langle i| \quad (1)$$

where $\varepsilon_i$ is the transition energy for dye $i$, which is 1.90 and 1.78 eV for Cy5 and Cy5.5, respectively (see, e.g., Figure 2A).

We proceeded to examine whether the purely electronic model could explain the progression of the transition energies associated with the most intense absorption of the tetramers, shown as black circles in Figure 4B. We first fit the data globally using a least-squares approach, varying only the excitonic hopping parameter to calculate the energy eigenvalues of the tetramer electronic transitions. We initially assumed no next-nearest-neighbor coupling (i.e., $J_{NN} = 0$). We found that the best fit is achieved for a $J_N$ value of 129 meV, which produces an average error of 0.7% between the measured transition energies and fitted energy eigenvalues. We then performed the global fit assuming the next-nearest-neighbor coupling is present (i.e., $J_{NN} = 2^{-3/2} \times J_N$). Since the nearest-neighbor and next-nearest-neighbor couplings are related by a coefficient, the global fit still uses a single fitting parameter. The best global fit was produced for a $J_N$ value of 108 meV, which produced the equivalent average error as when assuming $J_{NN} = 0$ (Figure 4B, orange). The global fit shown in Figure 4B agrees particularly well with the measured highest energy electronic transitions for the heterotetramers, but under- and overestimates the transition energies of the Cy5 and Cy5.5 homotetramers, respectively.

We then proceeded to fit the highest energy transitions for each tetramer type individually. This fit is shown in dotted green in Figure 4B. While there are no errors associated with these fits, it is useful to compare the calculated $J_N$ and $J_{NN}$ values, which are shown in Table 2. According to this model,

**Table 2. Exciton Hopping Parameters that Produced the Best Fit of the Highest Transition Energies of the Homo- and Heterotetramers via the Purely Electronic Exciton Theory Model**

| construct | $J_N$ (meV) | $J_{NN}$ (meV) |
|---|---|---|
| $A_5B_5C_5D_5$ | 123 | 43 |
| $A_5B_5C_5D_{5.5}$ | 111 | 39 |
| $A_5B_5C_{5.5}D_{5.5}$ | 110 | 39 |
| $A_5B_{5.5}C_5D_{5.5}$ | 110 | 39 |
| $A_5B_{5.5}C_{5.5}D_{5.5}$ | 105 | 37 |
| $A_{5.5}B_{5.5}C_{5.5}D_{5.5}$ | 92 | 33 |


https://doi.org/10.1021/acs.jpcc.2c04336
J. Phys. Chem. C 2022, 126, 17164−17175

the coupling between adjacent dyes exhibits a maximum value of 123 meV for the Cy5 homotetramer, decreases to a value of ∼110 meV for the heterotetramers and is independent of composition, and further decreases to a value of 92 meV for the Cy5.5 homotetramer. A possible explanation for this trend may be due to the extra bulkiness (i.e., aryl groups) associated with Cy5.5 in the heterotetramers and Cy5.5 homotetramer preventing the dyes from packing as close. The ability of this model to fit the highest energy transitions for all tetramers with a single fitting parameter suggests that the assumptions of the model are physically reasonable. For example, the good match of the exciton theory model with the data suggests that excitonic interactions between dyes are largely mediated by electronic rather than vibronic coupling.

To gain additional insight into the results of the purely electronic exciton theory model, we simulated the optical properties of the tetramers using a deeper level of theory. Specifically, we simulated the steady-state absorption and CD spectra via a model based on KRM theory.[61] In the KRM modeling approach, the best fit to the steady-state absorption and CD spectra is found by simulating a range of dye orientations within the aggregate.[45,57] The KRM modeling approach calculates $J_{mn}$ between every pair of dyes within the aggregate, models the TDMs as extended dipoles, and incorporates vibronic coupling to a single mode, making a comparison of the results of the KRM modeling an excellent test for the validity of the assumptions inherent to the exciton theory model. In the KRM modeling approach employed here, the centers of the extended dipoles were constrained to a square configuration, while the zenith and azimuthal angles were allowed to vary. The procedure was iterated to determine optimal dye separation (i.e., the edge length of the square configuration). Section S11 overlays the steady-state absorption and CD spectra of the Cy5 and Cy5.5 homotetramers with fits from the KRM modeling. Table 3 displays the associated $J_N$ and $J_{NN}$ values.

**Table 3. Excitonic Hopping Parameters of the Homotetramers Derived from KRM Modeling**

| construct | $J_N$ (meV) | $J_{NN}$ (meV) |
|---|---|---|
| $A_5B_5C_5D_5$ | 106 | 69 |
| $A_{5.5}B_{5.5}C_{5.5}D_{5.5}$ | 70 | 20 |

We then compared the results of KRM modeling to those of the purely electronic exciton model. For the Cy5 homotetramer, we find that the $J_N$ values in Table 2 (purely electronic model) are consistent with the corresponding values in Table 3 (KRM modeling approach), indicating good agreement between the two approaches. Interestingly, the $J_N$ value derived via the purely electronic model is slightly larger (∼16%) than the value derived via the KRM modeling approach, while $J_{NN}$ is appreciably smaller (∼38%). We explain the discrepancy in $J_{NN}$ values by considering that the excitonic coupling experienced between the extended dipoles used in KRM exhibits more gradual drop off at close range compared to the purely electronic model, which treats the TDMs as point dipoles. For the Cy5.5 homotetramer, $J_N$ and $J_{NN}$ values derived for the purely electronic model are ∼31 and ∼65% larger than the values derived by the KRM model, respectively.

Next, we compared the dye packing configurations of the two models. While the symmetry of the Hamiltonian matrix used in the purely electronic model implies the dyes are oriented perfectly parallel, the results of the KRM modeling indicate that the TDM vectors deviate somewhat from this ideal configuration. This deviation captures the circular dichroism exhibited by the tetramers. For the Cy5 homotetramer, this deviation is relatively small, and the average deviation from parallel for each pair of dyes is ∼17° (Section S11). For the Cy5.5 homotetramer, however, the TDM vectors deviated more appreciably, with an average deviation from parallel of ∼51°. The greater deviation from parallel calculated for the Cy5.5 homotetramer is consistent with its more complicated and intense CD response compared to the Cy5 homotetramer, which may also account for the greater deviation from the $J_{NN}$ predicted by the purely electronic model. Based on the agreement between the results of the KRM and the purely electronic models, we conclude that the dyes in the homotetramers pack approximately in the configuration of a square and that the assumptions inherent to the purely electronic model are sufficiently valid to enable basic predictions of the electronic structure of the Cy5 and Cy5.5 homo- and heterotetramers (for additional details and discussion, see, e.g., Section S12).

**Idealized J-Aggregate FRET Relay.** Our finding that the electronic structure of Cy5 and Cy5.5 homo- and heteroaggregate tetramers can be tuned by changing the aggregate composition, and that the resulting spectral variations are well described by a purely electronic exciton theory model, has interesting implications, particularly when extended to J-aggregates. The properties of J-aggregates, specifically their intense and narrow absorption bands and increased radiative rates relative to monomers,[18,19,62] are of interest for applications that involve EET. If the cyanine dyes Cy5 and Cy5.5 could be assembled in the form of J-aggregates of varying composition, the resultant material could potentially find application in organic optoelectronics, light harvesting, and nanoscale computing, as discussed in the Introduction.

To illustrate the potential impact of our results on EET, we next discuss how a FRET relay comprised of tunable J-aggregate heterotetramers might function. This idealized energy relay (Figure 5A) begins with a Cy5.5 monomer, includes three bridging Cy5 and Cy5.5 homo- and heterotetramers, and ends with a Cy5−Cy5.5 heterotetramer. Using the purely electronic exciton theory model as it would apply to the J-aggregate geometry, we calculated the transition energies using the Hamiltonian

$$\hat{H} = \sum_{n=0}^{3} \varepsilon_n |n\rangle\langle n| + \sum_{n=m\pm1}^{3} J_N |n\rangle\langle m| \quad (2)$$

where we assumed a $J_n$ value of 120 meV because it is comparable to the values derived for the H-aggregate homo- and heterotetramers. The calculated transition energies, in this case corresponding to the fully allowed lowest energy electronic transition, are shown above the corresponding J-aggregate homo- and heterotetramers in Figure 5. The tetramers are organized to spatially direct the EET; that is, EET proceeds downhill in energy from left-to-right in the diagram. To estimate the rates and efficiencies of EET in the FRET relay, we next simulated the optical spectra of the J-aggregate homo- and heterotetramers to extract the radiative rates of each tetramer and the absorption and emission spectral overlap integrals, which determine the EET rates.[17] Implicit in the calculated radiative rates is the assumption that the TDMs associated with each dye in the tetramer interact cooperatively,


https://doi.org/10.1021/acs.jpcc.2c04336
J. Phys. Chem. C 2022, 126, 17164−17175

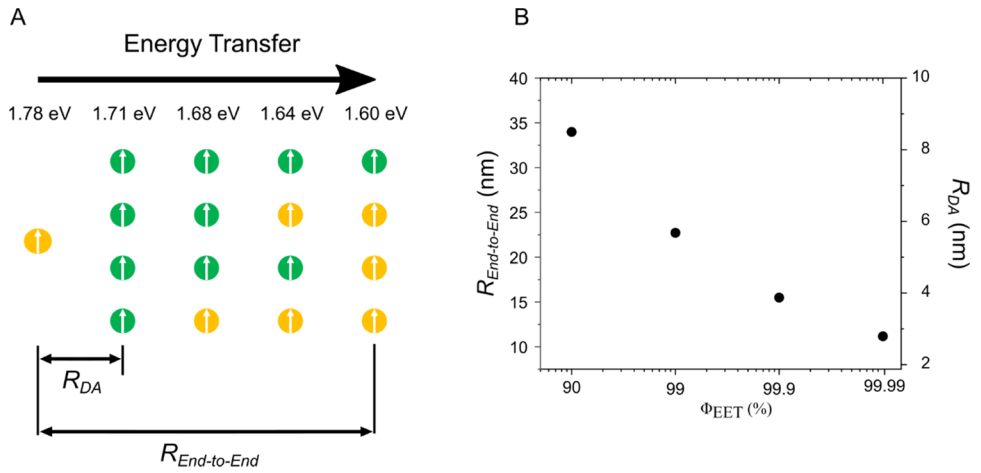


**Figure 5.** (A) Schematic diagram of the idealized J-aggregate FRET relay. Cy5 and Cy5.5 dyes are shown in green and yellow, respectively. The relay begins with Cy5.5 monomer, includes three intermediate homo- and heterotetramer J-aggregates, and ends with a heterotetramer J-aggregate. The energy value for Cy5.5 corresponds to 1.78 eV; shown above each homo- and heterotetramer is the calculated energy corresponding to the lowest energy electronic transition. Transition dipole moments of the constituent dyes are indicated by white arrows. Double headed arrows labeled $R_{DA}$ and $R_{End\text{-}to\text{-}End}$ indicate donor−acceptor and end-to-end distances, respectively. (B) Calculated $R_{DA}$ and $R_{End\text{-}to\text{-}End}$ as a function of electronic energy-transfer quantum efficiency (i.e., $\Phi_{EET}$).

i.e., the tetramers exhibit superradiance,[62,63] which is a potential advantage of using J-aggregates for EET. Additionally, the tunability of heteroaggregates can potentially be used to optimize spectral overlap integrals. For specified end-to-end EET quantum efficiencies, $\Phi_{EET}$, we calculated EET rates and maximum separations for the different donor−acceptor pairs (Section S13).

Figure 5B shows the relationship between the calculated maximum end-to-end distances and quantum efficiencies for the FRET relay. The results of these calculations have relevance to a number of applications based on EET. For example, the overall device efficiency of organic solar cells is often limited by the exciton diffusion length (typically ∼10 nm), which is generally an order of magnitude smaller than the absorption length (i.e., ∼100 nm).[64−66] Long-range spatially directed energy transfer up to 34 nm with an efficiency of 90% may benefit organic solar cells by facilitating spatially directed EET toward an electron donor/acceptor interface.[67] Figure 5B shows that a larger efficiency of 99% is achieved for a smaller distance of ∼23 nm, which may benefit light-harvesting systems where it has been suggested that large spatial separation of antenna complexes and reaction centers (i.e., greater than 10 nm) may prevent excitation quenching via chemical oxidation.[68] Even higher EET quantum efficiencies are possible for smaller end-to-end distances (although we acknowledge that deviations from the point-dipole approximation in this regime may cause quantitative disagreement[13,14,69]—see, e.g., Section S14). Higher EET efficiencies may benefit applications in nanoscale computing,[4] which are envisioned to include optical inputs, active elements, and optical outputs where EET mediates the transfer of excitons. For example, 99.9 and 99.99% quantum efficiencies, which result in end-to-end distances >10 nm, correspond to error rates of 1 in 1000 and 1 in 10 000, where the exciton does not transfer to the end of the relay. Such error rates are clearly within the 1% error permitted by computational error correction procedures.[70−73] The potential impact of such an idealized FRET relay on the applications highlighted above sheds promising light on the future utility of tunable heteroaggregates.

## CONCLUSIONS

In conclusion, we showed that the electronic structure of tetramer aggregates of two chemically distinct cyanine dyes is progressively tunable by modifying the aggregate composition. Specifically, we used DNA Holliday junctions to template homo- and heterotetramer aggregates of Cy5 and Cy5.5. The optical properties, including absorption and CD, exhibit a progressive trend with respect to Cy5.5 content; the overall blue shift of the absorption spectra was consistent with similar H-aggregate packing across the series. The aggregates in this form exhibited quenched fluorescence emission and short excited-state lifetimes. We applied an exciton theory model to describe the progression of the electronic structure, which had a number of assumptions including purely electronic interactions. The agreement between the experimental results, the purely electronic exciton theory model, and more advanced modeling based on KRM theory validated these assumptions. We proceeded to use the purely electronic exciton theory model to estimate end-to-end distances and overall EET quantum efficiencies for an idealized J-aggregate-based homo- and heterotetramer relay. If such FRET relays can be realized, they would have profound implications in a diverse range of fields including light harvesting, organic optoelectronics, and nanoscale computing.

## ASSOCIATED CONTENT

### Supporting Information

The Supporting Information is available free of charge at https://pubs.acs.org/doi/10.1021/acs.jpcc.2c04336.

Methods, additional steady-state absorption, circular dichroism, and fluorescence spectroscopy, additional transient absorption and time-resolved fluorescence spectroscopy, and additional theoretical calculation and simulation (PDF)

## AUTHOR INFORMATION

### Corresponding Authors

**Daniel B. Turner** − *Micron School of Materials Science & Engineering, Boise State University, Boise, Idaho 83725,*



https://doi.org/10.1021/acs.jpcc.2c04336
J. Phys. Chem. C 2022, 126, 17164−17175

*United States;* orcid.org/0000-0002-3148-5317; Email: danielturner926@boisestate.edu

**Joseph S. Melinger** − *Electronics Science and Technology Division Code 6800, U.S. Naval Research Laboratory, Washington, District of Columbia 20375, United States;* orcid.org/0000-0002-2452-5245; Email: joseph.melinger@nrl.navy.mil

**Ryan D. Pensack** − *Micron School of Materials Science & Engineering, Boise State University, Boise, Idaho 83725, United States;* orcid.org/0000-0002-1302-1770; Email: ryanpensack@boisestate.edu

## Authors

**Jonathan S. Huff** − *Micron School of Materials Science & Engineering, Boise State University, Boise, Idaho 83725, United States;* orcid.org/0000-0002-2025-9605

**Sebastián A. Díaz** − *Center for Bio/Molecular Science and Engineering Code 6900, U.S. Naval Research Laboratory, Washington, District of Columbia 20375, United States;* orcid.org/0000-0002-5568-0512

**Matthew S. Barclay** − *Micron School of Materials Science & Engineering, Boise State University, Boise, Idaho 83725, United States*

**Azhad U. Chowdhury** − *Micron School of Materials Science & Engineering, Boise State University, Boise, Idaho 83725, United States*

**Matthew Chiriboga** − *Center for Bio/Molecular Science and Engineering Code 6900, U.S. Naval Research Laboratory, Washington, District of Columbia 20375, United States; Volgenau School of Engineering, George Mason University, Fairfax, Virginia 22030, United States*

**Gregory A. Ellis** − *Center for Bio/Molecular Science and Engineering Code 6900, U.S. Naval Research Laboratory, Washington, District of Columbia 20375, United States*

**Divita Mathur** − *Center for Bio/Molecular Science and Engineering Code 6900, U.S. Naval Research Laboratory, Washington, District of Columbia 20375, United States; College of Science, George Mason University, Fairfax, Virginia 22030, United States;* orcid.org/0000-0002-3537-7292

**Lance K. Patten** − *Micron School of Materials Science & Engineering, Boise State University, Boise, Idaho 83725, United States;* orcid.org/0000-0003-4846-2207

**Simon K. Roy** − *Micron School of Materials Science & Engineering, Boise State University, Boise, Idaho 83725, United States;* orcid.org/0000-0001-8652-1277

**Aaron Sup** − *Department of Physics, Boise State University, Boise, Idaho 83725, United States*

**Austin Biaggne** − *Micron School of Materials Science & Engineering, Boise State University, Boise, Idaho 83725, United States*

**Brian S. Rolczynski** − *Electronics Science and Technology Division Code 6800, U.S. Naval Research Laboratory, Washington, District of Columbia 20375, United States;* orcid.org/0000-0002-8783-1266

**Paul D. Cunningham** − *Electronics Science and Technology Division Code 6800, U.S. Naval Research Laboratory, Washington, District of Columbia 20375, United States;* orcid.org/0000-0002-3602-1503

**Lan Li** − *Micron School of Materials Science & Engineering, Boise State University, Boise, Idaho 83725, United States; Center for Advanced Energy Studies, Idaho Falls, Idaho 83401, United States*

**Jeunghoon Lee** − *Micron School of Materials Science & Engineering and Department of Chemistry & Biochemistry, Boise State University, Boise, Idaho 83725, United States;* orcid.org/0000-0002-1909-4591

**Paul H. Davis** − *Micron School of Materials Science & Engineering, Boise State University, Boise, Idaho 83725, United States; Center for Advanced Energy Studies, Idaho Falls, Idaho 83401, United States;* orcid.org/0000-0001-7333-8748

**Bernard Yurke** − *Micron School of Materials Science & Engineering and Department of Electrical & Computer Engineering, Boise State University, Boise, Idaho 83725, United States;* orcid.org/0000-0003-3913-2855

**William B. Knowlton** − *Micron School of Materials Science & Engineering and Department of Electrical & Computer Engineering, Boise State University, Boise, Idaho 83725, United States;* orcid.org/0000-0003-3018-2207

**Igor L. Medintz** − *Center for Bio/Molecular Science and Engineering Code 6900, U.S. Naval Research Laboratory, Washington, District of Columbia 20375, United States;* orcid.org/0000-0002-8902-4687

Complete contact information is available at: https://pubs.acs.org/10.1021/acs.jpcc.2c04336

## Notes

The authors declare no competing financial interest.

## ■ ACKNOWLEDGMENTS

Research at Boise State was supported by the Department of the Navy, Office of Naval Research (ONR) via ONR award no. N00014-19-1-2615. Research at the U.S. Naval Research Laboratory (NRL) was supported by NRL base funding, the NRL Institute for Nanoscience, and ONR award # N0001419WX01811. D.M. was supported by the National Institute of Biomedical Imaging and Bioengineering of the National Institutes of Health under award number K99EB030013. The content is solely the responsibility of the authors and does not necessarily represent the official views of the National Institutes of Health. The femtosecond fluorescence spectrometer was made available through the U.S. Department of Energy, Office of Basic Energy Sciences, Division of Materials Science and Engineering through the Established Program to Stimulate Competitive Research (EPSCoR) via award no. DE-SC0020089.

## ■ REFERENCES

(1) Mirkovic, T.; Ostroumov, E. E.; Anna, J. M.; van Grondelle, R.; Scholes, G. D. Light Absorption and Energy Transfer in the Antenna Complexes of Photosynthetic Organisms. *Chem. Rev.* **2017**, *117*, 249−293.

(2) Brixner, T.; Hildner, R.; Köhler, J.; Lambert, C.; Würthner, F. Exciton Transport in Molecular Aggregates − From Natural Antennas to Synthetic Chromophore Systems. *Adv. Energy Mater.* **2017**, *7*, 1−33.

(3) Ostroverkhova, O. Organic Optoelectronic Materials: Mechanisms and Applications. *Chem. Rev.* **2016**, *116*, 13279−13412.

(4) Yurke, B.; Kuang, W. Passive Linear Nanoscale Optical and Molecular Electronics Device Synthesis from Nanoparticles. *Phys. Rev. A* **2010**, *81*, 033814−1−9.

(5) Graugnard, E.; Kellis, D. L.; Bui, H.; Barnes, S.; Kuang, W.; Lee, J.; Hughes, W. L.; Knowlton, W. B.; Yurke, B. DNA-Controlled Excitonic Switches. *Nano Lett.* **2012**, *12*, 2117−2122.

(6) Laboda, C.; Duschl, H.; Dwyer, C. L. DNA-Enabled Integrated Molecular Systems for Computation and Sensing. *Acc. Chem. Res.* **2014**, *47*, 1816−1824.
(7) Cannon, B. L.; Kellis, D. L.; Davis, P. H.; Lee, J.; Kuang, W.; Hughes, W. L.; Graugnard, E.; Yurke, B.; Knowlton, W. B. Excitonic AND Logic Gates on DNA Brick Nanobreadboards. *ACS Photonics* **2015**, *2*, 398−404.
(8) Sawaya, N. P. D.; Rappoport, D.; Tabor, D. P.; Aspuru-Guzik, A. Excitonics: A Set of Gates for Molecular Exciton Processing and Signaling. *ACS Nano* **2018**, *12*, 6410−6420.
(9) Kellis, D. L.; Sarter, C.; Cannon, B. L.; Davis, P. H.; Graugnard, E.; Lee, J.; Pensack, R. D.; Kolmar, T.; Jäschke, A.; Yurke, B.; Knowlton, W. B. An All-Optical Excitonic Switch Operated in the Liquid and Solid Phases. *ACS Nano* **2019**, *13*, 2986−2994.
(10) Castellanos, M. A.; Dodin, A.; Willard, A. P. On the Design of Molecular Excitonic Circuits for Quantum Computing: The Universal Quantum Gates. *Phys. Chem. Chem. Phys.* **2020**, *22*, 3048−3057.
(11) Förster, T. Energiewanderung Und Fluoreszenz. *Naturwissenschaften* **1946**, *33*, 166−175.
(12) Förster, T. Energy Migration and Fluorescence. *J. Biomed. Opt.* **2012**, *17*, No. 011002.
(13) Muñoz-Losa, A.; Curutchet, C.; Krueger, B. P.; Hartsell, L. R.; Mennucci, B. Fretting about FRET: Failure of the Ideal Dipole Approximation. *Biophys. J.* **2009**, *96*, 4779−4788.
(14) Scholes, G. D. Designing Light-Harvesting Antenna Systems Based on Superradiant Molecular Aggregates. *Chem. Phys.* **2002**, *275*, 373−386.
(15) Petkov, B. K.; Gellen, T. A.; Farfan, C. A.; Carbery, W. P.; Hetzler, B. E.; Trauner, D.; Li, X.; Glover, W. J.; Ulness, D. J.; Turner, D. B. Two-Dimensional Electronic Spectroscopy Reveals the Spectral Dynamics of Förster Resonance Energy Transfer. *Chem* **2019**, *5*, 2111−2125.
(16) Scholes, G. D. Long-Range Resonance Energy Transfer in Molecular Systems. *Annu. Rev. Phys. Chem.* **2003**, *54*, 57−87.
(17) Clegg, R. M. Fluorescence Resonance Energy Transfer and Nucleic Acids. *Methods Enzymol.* **1992**, *211*, 353−388.
(18) Würthner, F.; Kaiser, T. E.; Saha-Möller, C. R. J-Aggregates: From Serendipitous Discovery to Supramolecular Engineering of Functional Dye Materials. *Angew. Chem., Int. Ed.* **2011**, *50*, 3376−3410.
(19) Bricks, J. L.; Slominskii, Y. L.; Panas, I. D.; Demchenko, A. P. Fluorescent J-Aggregates of Cyanine Dyes: Basic Research and Applications Review. *Methods Appl. Fluoresc.* **2017**, *6*, No. 012001.
(20) Mirkovic, T.; Ostroumov, E. E.; Anna, J. M.; van Grondelle, R.; Govindjee; Scholes, G. D. Light Absorption and Energy Transfer in the Antenna Complexes of Photosynthetic Organisms. *Chem. Rev.* **2017**, *117*, 249−293.
(21) Kasha, M. Energy Transfer Mechanisms and the Molecular Exciton Model for Molecular Aggregates. *Radiat. Res.* **1963**, *20*, 55−70.
(22) Kasha, M.; Rawls, H. R.; Ashraf El-Bayoumi, M. The Exciton Model in Molecular Spectroscopy. *Pure Appl. Chem.* **1965**, *11*, 371−392.
(23) McRae, E. G.; Kasha, M. Enhancement of Phosphorescence Ability upon Aggregation of Dye Molecules. *J. Chem. Phys.* **1958**, *28*, 722.
(24) Turro, N. J.; Scaiano, J. C.; Ramamurthy, V. *Modern Molecular Photochemistry of Organic Molecules*; University Science Books: Sausalito, California, 2010.
(25) Kashida, H.; Fujii, T.; Asanuma, H. Threoninol as a Scaffold of Dyes (Threoninol-Nucleotide) and Their S′ Interstrand Clustering in Duplexes. *Org. Biomol. Chem* **2008**, *6*, 2892−2899.
(26) Kirchner, E.; Bialas, D.; Fennel, F.; Grüne, M.; Würthner, F. Defined Merocyanine Dye Stacks from a Dimer up to an Octamer by Spacer-Encoded Self-Assembly Approach. *J. Am. Chem. Soc.* **2019**, *141*, 7428−7438.
(27) Ahn, T. S.; Müller, A. M.; Al-Kaysi, R. O.; Spano, F. C.; Norton, J. E.; Beljonne, D.; Brédas, J. L.; Bardeen, C. J. Experimental and Theoretical Study of Temperature Dependent Exciton Delocalization and Relaxation in Anthracene Thin Films. *J. Chem. Phys.* **2008**, *128*, No. 054505.
(28) Seeman, N. C.; Kallenbach, N. R. Design of Immobile Nucleic Acid Junctions. *Biophys. J.* **1983**, *44*, 201−209.
(29) Brown, C. W.; Buckhout-White, S.; Díaz, S. A.; Melinger, J. S.; Ancona, M. G.; Goldman, E. R.; Medintz, I. L. Evaluating Dye-Labeled DNA Dendrimers for Potential Applications in Molecular Biosensing. *ACS Sens.* **2017**, *2*, 401−410.
(30) Olshansky, J. H.; Zhang, J.; Krzyaniak, M. D.; Lorenzo, E. R.; Wasielewski, M. R. Selectively Addressable Photogenerated Spin Qubit Pairs in DNA Hairpins. *J. Am. Chem. Soc.* **2020**, *142*, 3346−3350.
(31) Depew, D. E.; Wang, J. C. Conformational Fluctuations of DNA Helix. *Proc. Natl. Acad. Sci. U.S.A.* **1975**, *72*, 4275−4279.
(32) Rothemund, P. W. K. Folding DNA to Create Nanoscale Shapes and Patterns. *Nature* **2006**, *440*, 297−302.
(33) Bösch, C. D.; Jevric, J.; Bürki, N.; Probst, M.; Langenegger, S. M.; Häner, R. Supramolecular Assembly of DNA-Phenanthrene Conjugates into Vesicles with Light-Harvesting Properties. *Bioconjugate Chem.* **2018**, *29*, 1505−1509.
(34) Rothenbühler, S.; Iacovache, I.; Langenegger, S. M.; Zuber, B.; Häner, R. Complex DNA Architectonics—Self-Assembly of Amphiphilic Oligonucleotides into Ribbons, Vesicles, and Asterosomes *Bioconjugate Chem.*, **2022**, DOI: 10.1021/acs.bioconjchem.2c00077.
(35) Nicoli, F.; Roos, M. K.; Hemmig, E. A.; Di Antonio, M.; De Vivie-Riedle, R.; Liedl, T. Proximity-Induced H-Aggregation of Cyanine Dyes on DNA-Duplexes. *J. Phys. Chem. A* **2016**, *120*, 9941−9947.
(36) Cunningham, P. D.; Kim, Y. C.; Díaz, S. A.; Buckhout-White, S.; Mathur, D.; Medintz, I. L.; Melinger, J. S. Optical Properties of Vibronically Coupled Cy3 Dimers on DNA Scaffolds. *J. Phys. Chem. B* **2018**, *122*, 5020−5029.
(37) Heussman, D.; Kittell, J.; Kringle, L.; Tamimi, A.; von Hippel, P. H.; Marcus, A. H. Measuring Local Conformations and Conformational Disorder of $(Cy3)_2$ Dimer Labeled DNA Fork Junctions Using Absorbance, Circular Dichroism and Two-Dimensional Fluorescence Spectroscopy. *Faraday Discuss.* **2019**, *216*, 211−235.
(38) Cunningham, P. D.; Díaz, S. A.; Yurke, B.; Medintz, I. L.; Melinger, J. S. Delocalized Two-Exciton States in DNA Scaffolded Cyanine Dimers. *J. Phys. Chem. B* **2020**, *124*, 8042−8049.
(39) Mass, O. A.; Wilson, C. K.; Roy, S. K.; Barclay, M. S.; Patten, L. K.; Terpetschnig, E. A.; Lee, J.; Pensack, R. D.; Yurke, B.; Knowlton, W. B. Exciton Delocalization in Indolenine Squaraine Aggregates Templated by DNA Holliday Junction Scaffolds. *J. Phys. Chem. B* **2020**, *124*, 9636−9647.
(40) Hart, S. M.; Chen, W. J.; Banal, J. L.; Bricker, W. P.; Dodin, A.; Markova, L.; Vyborna, Y.; Willard, A. P.; Häner, R.; Bathe, M.; Schlau-Cohen, G. S. Engineering Couplings for Exciton Transport Using Synthetic DNA Scaffolds. *Chem* **2021**, *7*, 752−773.
(41) Mass, O. A.; Wilson, C. K.; Barcenas, G.; Terpetschnig, E. A.; Obukhova, O. M.; Kolosova, O. S.; Tatarets, A. L.; Li, L.; Yurke, B.; Knowlton, W. B.; et al. Influence of Hydrophobicity on Excitonic Coupling in DNA-Templated Indolenine Squaraine Dye Aggregates. *J. Phys. Chem. C* **2022**, *126*, 3475−3488.
(42) Hart, S. M.; Wang, X.; Guo, J.; Bathe, M.; Schlau-Cohen, G. S. Tuning Optical Absorption and Emission Using Strongly Coupled Dimers in Programmable DNA Scaffolds. *J. Phys. Chem. Lett.* **2022**, *13*, 1863−1871.
(43) Chowdhury, A. U.; Díaz, S. A.; Huff, J. S.; Barclay, M. S.; Chiriboga, M.; Ellis, G. A.; Mathur, D.; Patten, L. K.; Sup, A.; Hallstrom, N.; et al. Tuning between Quenching and Energy Transfer in DNA-Templated Heterodimer Aggregates. *J. Phys. Chem. Lett.* **2022**, *13*, 2782−2791.
(44) Barclay, M. S.; Wilson, C. K.; Roy, S. K.; Mass, O. A.; Obukhova, O. M.; Svoiakov, R. P.; Tatarets, A. L.; Chowdhury, A. U.; Huff, J. S.; Turner, D. B.; et al. Oblique Packing and Tunable Excitonic Coupling in DNA-Templated Squaraine Rotaxane Dimer Aggregates. *ChemPhotoChem* **2022**, *6*, No. e202200039.

(45) Cannon, B. L.; Kellis, D. L.; Patten, L. K.; Davis, P. H.; Lee, J.; Graugnard, E.; Yurke, B.; Knowlton, W. B. Coherent Exciton Delocalization in a Two-State DNA-Templated Dye Aggregate System. *J. Phys. Chem. A* **2017**, *121*, 6905−6916.
(46) Markova, L. I.; Malinovskii, V. L.; Patsenker, L. D.; Häner, R. J-vs. H-Type Assembly: Pentamethine Cyanine (Cy5) as a near-IR Chiroptical Reporter. *Chem. Commun.* **2013**, *49*, 5298−5300.
(47) Heussman, D.; Kittell, J.; Von Hippel, P. H.; Marcus, A. H. Temperature-Dependent Local Conformations and Conformational Distributions of Cyanine Dimer Labeled Single-Stranded-Double-Stranded DNA Junctions by 2D Fluorescence Spectroscopy. *J. Chem. Phys.* **2022**, *156*, No. 045101.
(48) Fujii, T.; Kashida, H.; Asanuma, H. Analysis of Coherent Heteroclustering of Different Dyes by Use of Threoninol Nucleotides for Comparison with the Molecular Exciton Theory. *Chem. - Eur. J.* **2009**, *15*, 10092−10102.
(49) Asanuma, H.; Fujii, T.; Kato, T.; Kashida, H. Coherent Interactions of Dyes Assembled on DNA. *J. Photochem. Photobiol., C* **2012**, *13*, 124−135.
(50) Asanuma, H.; Murayama, K.; Kamiya, Y.; Kashida, H. The DNA Duplex as an Aqueous One-Dimensional Soft Crystal Scaffold for Photochemistry. *Bull. Chem. Soc. Jpn.* **2018**, *91*, 1739−1748.
(51) Biaggne, A.; Spear, L.; Barcenas, G.; Ketteridge, M.; Kim, Y. C.; Melinger, J. S.; Knowlton, W. B.; Yurke, B.; Li, L. Data-Driven and Multiscale Modeling of DNA-Templated Dye Aggregates. *Molecules* **2022**, *27*, No. 3456.
(52) Meares, A.; Susumu, K.; Mathur, D.; Lee, S. H.; Mass, O. A.; Lee, J.; Pensack, R. D.; Yurke, B.; Knowlton, W. B.; Melinger, J. S.; Medintz, I. L. Synthesis of Substituted Cy5 Phosphoramidite Derivatives and Their Incorporation into Oligonucleotides Using Automated DNA Synthesis. *ACS Omega* **2022**, *7*, 11002−11016.
(53) Mustroph, H.; Reiner, K.; Mistol, J.; Ernst, S.; Keil, D.; Hennig, L. Relationship between the Molecular Structure of Cyanine Dyes and the Vibrational Fine Structure of Their Electronic Absorption Spectra. *ChemPhysChem* **2009**, *10*, 835−840.
(54) Bishop, M. M.; Roscioli, J. D.; Ghosh, S.; Mueller, J. J.; Shepherd, N. C.; Beck, W. F. Vibrationally Coherent Preparation of the Transition State for Photoisomerization of the Cyanine Dye Cy5 in Water. *J. Phys. Chem. B* **2015**, *119*, 6905−6915.
(55) Spiegel, J. D.; Fulle, S.; Kleinschmidt, M.; Gohlke, H.; Marian, C. M. Failure of the IDA in FRET Systems at Close Inter-Dye Distances Is Moderated by Frequent Low K2 Values. *J. Phys. Chem. B* **2016**, *120*, 8845−8862.
(56) Biaggne, A.; Knowlton, W. B.; Yurke, B.; Lee, J.; Li, L. Substituent Effects on the Solubility and Electronic Properties of the Cyanine Dye Cy5: Density Functional and Time-Dependent Density Functional Theory Calculations. *Molecules* **2021**, *26*, No. 524.
(57) Cannon, B. L.; Patten, L. K.; Kellis, D. L.; Davis, P. H.; Lee, J.; Graugnard, E.; Yurke, B.; Knowlton, W. B. Large Davydov Splitting and Strong Fluorescence Suppression: An Investigation of Exciton Delocalization in DNA-Templated Holliday Junction Dye Aggregates. *J. Phys. Chem. A* **2018**, *122*, 2086−2095.
(58) Huff, J. S.; Davis, P. H.; Christy, A.; Kellis, D. L.; Kandadai, N.; Toa, Z. S. D.; Scholes, G. D.; Yurke, B.; Knowlton, W. B.; Pensack, R. D. DNA-Templated Aggregates of Strongly Coupled Cyanine Dyes: Nonradiative Decay Governs Exciton Lifetimes. *J. Phys. Chem. Lett.* **2019**, *10*, 2386−2392.
(59) Huff, J. S.; Turner, D. B.; Mass, O. A.; Patten, L. K.; Wilson, C. K.; Roy, S. K.; Barclay, M. S.; Yurke, B.; Knowlton, W. B.; Davis, P. H.; Pensack, R. D. Excited-State Lifetimes of DNA-Templated Cyanine Dimer, Trimer, and Tetramer Aggregates: The Role of Exciton Delocalization, Dye Separation, and DNA Heterogeneity. *J. Phys. Chem. B* **2021**, *125*, 10240−10259.
(60) Von Hippel, P. H.; Johnson, N. P.; Marcus, A. H. Fifty Years of DNA "Breathing": Reflections on Old and New Approaches. *Biopolymers* **2013**, *99*, 923−954.
(61) Kühn, O.; Renger, T.; May, V. Theory of Exciton-Vibrational Dynamics in Molecular Dimers. *Chem. Phys.* **1996**, *204*, 99−114.
(62) Spano, F. C.; Kuklinski, J. R.; Mukamel, S. Cooperative Radiative Dynamics in Molecular Aggregates. *J. Chem. Phys.* **1991**, *94*, 7534−7544.
(63) Dicke, R. H. Coherence in Spontaneous Radiation Process. *Phys. Rev.* **1954**, *93*, No. 99.
(64) Brédas, J.-L.; Norton, J.; Cornil, J. Molecular Understanding of Organic Solar Cells: The Challenges. *Acc. Chem. Res.* **2009**, *42*, 1691−1699.
(65) Clarke, T. M.; Durrant, J. R. Charge Photogeneration in Organic Solar Cells. *Chem. Rev.* **2010**, *110*, 6736−6767.
(66) Ostroverkhova, O. Organic Optoelectronic Materials: Mechanisms and Applications. *Chem. Rev.* **2016**, *116*, 13279−13412.
(67) Scully, S. R.; Armstrong, P. B.; Edder, C.; Fréchet, J. M. J.; McGehee, M. D. Long-Range Resonant Energy Transfer for Enhanced Exciton Harvesting for Organic Solar Cells. *Adv. Mater.* **2007**, *19*, 2961−2966.
(68) Sundström, V.; Pullerits, T.; Van Grondelle, R. Photosynthetic Light-Harvesting: Reconciling Dynamics and Structure of Purple Bacterial LH2 Reveals Function of Photosynthetic Unit. *J. Phys. Chem. B* **1999**, *103*, 2327−2346.
(69) Scholes, G. D.; Mirkovic, T.; Turner, D. B.; Fassioli, F.; Buchleitner, A. Solar Light Harvesting by Energy Transfer: From Ecology to Coherence. *Energy Environ. Sci.* **2012**, *5*, 9374−9393.
(70) Fowler, A. G.; Whiteside, A. C.; Hollenberg, L. C. L. Towards Practical Classical Processing for the Surface Code. *Phys. Rev. Lett.* **2012**, *108*, No. 180501.
(71) Fowler, A. G.; Mariantoni, M.; Martinis, J. M.; Cleland, A. N. Surface Codes: Towards Practical Large-Scale Quantum Computation. *Phys. Rev. A* **2012**, *86*, No. 032324.
(72) Wang, D. S.; Fowler, A. G.; Hollenberg, L. C. L. Surface Code Quantum Computing with Error Rates over 1%. *Phys. Rev. A* **2011**, *83*, No. 020302.
(73) Stephens, A. M. Fault-Tolerant Thresholds for Quantum Error Correction with the Surface Code. *Phys. Rev. A* **2014**, *89*, No. 022321.




https://doi.org/10.1021/acs.jpcc.2c04336
J. Phys. Chem. C 2022, 126, 17164−17175